Rapid Communications

Magnetoplasmonic enhancement of Faraday rotation in patterned graphene metasurfaces

Michele Tamagnone,[1,2,*] Tetiana M. Slipchenko,[3] Clara Moldovan,[4] Peter Q. Liu,[5] Alba Centeno,[6] Hamed Hasani,[1] Amaia Zurutuza,[6] Adrian M. Ionescu,[4] Luis Martin-Moreno,[3] Jérôme Faist,[7] Juan R. Mosig,[1] Alexey B. Kuzmenko,[8] and Jean-Marie Poumirol[8,†]

[1]*Laboratory of Electromagnetics and Antennas (LEMA), École Polytechnique Fédérale de Lausanne, EPFL, Station 11, 1015 Lausanne, Switzerland*

[2]*Harvard John A. Paulson School of Engineering and Applied Sciences, Harvard University, Cambridge, Massachusetts 02138, USA*

[3]*Instituto de Ciencia de Materiales de Aragon and Departamento de Fisica de la Materia Condensada, CSIC-Universidad de Zaragoza, E-50009 Zaragoza, Spain*

[4]*Nanoelectronic Devices Laboratory, Ecole Polytechnique Fédérale de Lausanne, Lausanne, Switzerland*

[5]*Department of Electrical Engineering, The State University of New York at Buffalo, Buffalo, New York 14260, USA*

[6]*Graphenea SA, E-20018 Donostia-San Sebastián, Spain*

[7]*Institute for Quantum Electronics, Department of Physics, ETH Zurich, CH-8093 Zurich, Switzerland*

[8]*Department of Quantum Matter Physics, University of Geneva, CH-1211 Geneva 4, Switzerland*

(Received 16 November 2017; published 26 June 2018)

Faraday rotation is a fundamental property present in all nonreciprocal optical elements. In the THz range, graphene displays strong Faraday rotation; unfortunately, it is limited to frequencies below the cyclotron resonance. Here, we show experimentally that in specifically designed metasurfaces, magnetoplasmons can be used to circumvent this limitation. We find excellent agreement between theory and experiment and provide physical insights and predictions on these phenomena. Finally, we demonstrate strong tunability in these metasurfaces using electric and magnetic field biasing.

DOI: 10.1103/PhysRevB.97.241410

Graphene is considered a very promising material for nonreciprocal magneto-optical applications at microwave, terahertz, and infrared frequencies [1–18]. Two of the most common nonreciprocal devices are isolators and circulators, and both are realizable starting from a Faraday rotator [9,11,16,19]. On top of a strong Faraday rotation (FR), graphene offers the possibility of tunability/modulability via a gate.

Unfortunately, Faraday rotation observed in uniform graphene typically exhibits a maximum at low frequency (<1 THz), and is barely present at higher frequencies, apparently precluding applications above 3 THz [3,4,12]. In nonuniform media, it was experimentally found that the magneto-optical response in transmission is enhanced at the plasmonic resonance frequency, in structures such as graphene dots [8], antidots [20], and ribbons [21], but the effect of magnetoplasmonic resonance on the FR remains experimentally unexplored. It was numerically demonstrated that such plasmonic structures should also induce a blueshifting of the Faraday rotation maximum [13,16], but the fundamental questions of how to preserve and manipulate FR above the cyclotron resonance are still open.

In continuous graphene, the impedance of the continuous monolayer is given for the two opposite circular polarizations by [5]

$$Z_{\pm} = \sigma_{\pm}^{-1} = \sigma_{\mathrm{dc}}^{-1}[1 + i\tau(\omega \pm \omega_{\mathrm{c}})], \tag{1}$$

where ω is the photon frequency, τ the carriers' scattering time, $\sigma_{\mathrm{dc}} = e^2\tau|E_{\mathrm{F}}|(\pi\hbar^2)^{-1}$ is the low-temperature low-frequency limit of graphene's conductivity for no magnetic bias, and $\omega_{\mathrm{c}} = ev_{\mathrm{f}}^2 B|E_{\mathrm{F}}|^{-1}$ is the semiclassical cyclotron frequency. In such a system the maximum FR always appears at energies below the cyclotron resonance. To go even further, when considering the highly doped (and/or low magnetic field regime) where τ^{-1} is dominant over ω_{c}, the Faraday rotation will peak at zero frequency and will not extend above a cutoff frequency given by $\omega = \tau^{-1}$, explaining the experimentally observed strong reduction of FR above 3 THz [3,4,12].

Trying to circumvent these limitations, in this Rapid Communication, we have studied both experimentally and numerically the behavior of the Faraday rotation in three different patterned structures: a periodic array of graphene square dots (GSDs), a graphene square antidot lattice (GSA), and a hybrid metal-graphene patterned structure (HMG). Circumventing the limitations observed in graphene, we have confirmed for all structures the presence of nonreciprocal magnetoplasmons blueshifting the Faraday rotation far above the cyclotron resonance. We went further by showing that each metasurface allows specific control over the frequency and broadening of the nonreciprocal optical responce of graphene.

All the samples measured in this Rapid Communication are made from chemical vapor deposited (CVD) graphene, transferred on oxidized high-resistivity silicon wafers (oxide thickness $t_{\mathrm{ox}} = 280$ nm). The different patterns studied here were made using a combination of *e*-beam lithography, oxygen plasma etching, and gold deposition. Infrared spectra were measured through a 3-mm-diam hole fully covered by the

*mtamagnone@seas.harvard.edu
†Jean-Marie.Poumirol@unige.ch

samples (5×5 mm^2), at room temperature ($T = 280$ K), in a split-coil superconducting magnet attached to a Fourier-transform infrared (FTIR) spectrometer. The resolution (4 cm^{-1}) was selected to remove the effect of the multiple reflection in the chip, equivalent to suppressing the phase coherence between multiple reflections. Following the procedure described in Ref. [22], for each magnetic field B, the Faraday angle $\theta_F(\omega)$ was measured using a two-polarizer configuration with a fixed polarizer and a mobile analyzer.

A scanning electron microscopy (SEM) image of the typical GSD is shown in Fig. 1(a). The pattern consists of periodic squares with a periodicity $P = 1$ μm and a distance between the dots $d = 150$ nm [5].

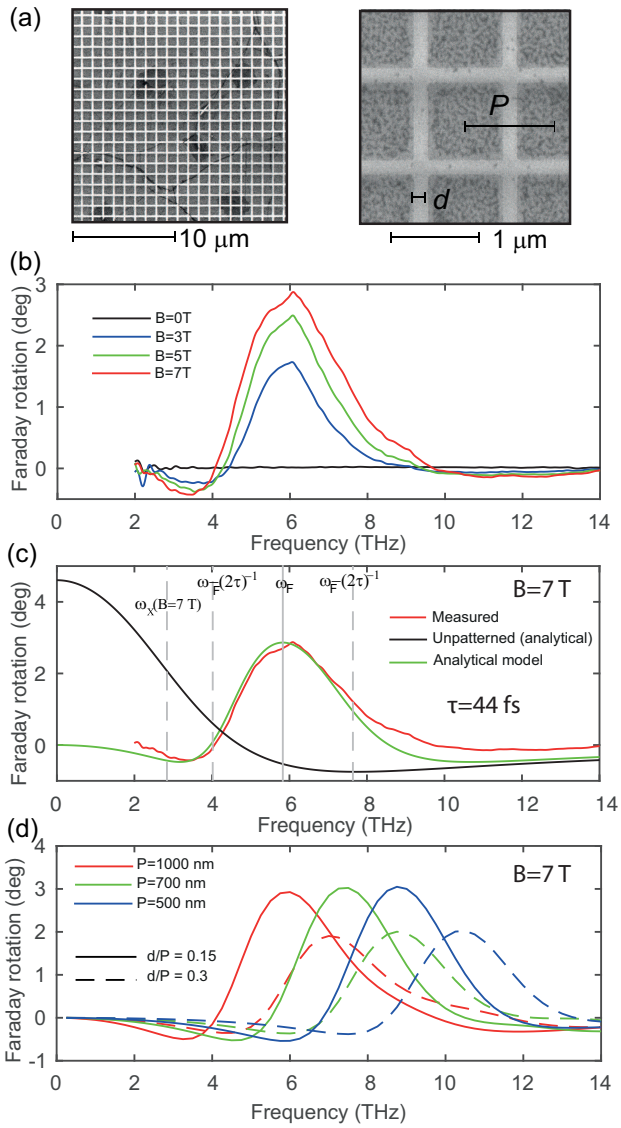

FIG. 1. (a) SEM pictures of the nanopatterned graphene square dot GSD lattice sample studied in this work. $P = 1$ μm, $d = 150$ nm. (b) Measured Faraday rotation on the GSD sample at several magnetic fields up to 7 T. (c) Comparison between experimental data and the analytically predicted FR for $B = 7$ T; expected broadening (central frequency) appears as a dotted (continuous) gray line. Expected ω_c in this system at $B = 7$ T is shown as a gray dashed line. (d) Full-wave simulations for various periods and fill ratios.

The FR measured in GSD is shown in Fig. 1(b) for several magnetic fields up to 7 T. One can see that $\theta_F(\omega)$ in this structure displays a very different behavior from the monotonous FR observed in continuous graphene and described above. For all nonzero magnetic fields $\theta_F(\omega)$ exhibits a bell-shaped curve, centered around 6 THz. The amplitude of the FR increases with the magnetic field B, but neither the broadening nor the position of this maximum are affected by the variation of B.

To understand this behavior we can generalize Eq. (1) for the patterned case. The biperiodic patterns of etched gaps have the function of interrupting the path of surface currents on graphene by adding a series capacitive term C_g, originating from the displacement currents. The impedance of the obtained graphene metasurface is then [23]

$$Z_{M\pm} = \frac{\pi\hbar^2}{e^2|E_F|p}\left[\tau^{-1} + i\left(\omega \pm \omega_c - \frac{e^2|E_F|}{\omega p \pi \hbar^2 C_g}\right)\right], \quad (2)$$

where $p = \frac{8}{\pi^2}(1 - \frac{d}{P})^2 < 1$ is the pattern filling factor, reducing the overall conductivity tensor [5]. p includes a current pattern factor $c_f = 8/\pi^2$ which models the approximately sinusoidal current density profile on the patch, which gradually tends to zero at the edges [24]. In analogy with continuous graphene, a good estimation for the frequency of maximum Faraday rotation in the low mobility regime is then found from the condition $\mathrm{Im}(Z_{M+}) + \mathrm{Im}(Z_{M-}) = 0$, where Z_{M+} and Z_{M-} have the same modulus but the phase difference is maximized,

$$\omega_F = \frac{e}{\hbar}\sqrt{\frac{E_F}{\pi p C_g}}, \quad (3)$$

providing a nonzero resonance value depending on the Fermi level and the chosen pattern but not on the magnetic field, as observed experimentally. ω_F can be understood as a plasmonic resonance arising between the kinetic inductance $L_k = e^2|E_F|(\pi\hbar^2)^{-1}$ of graphene and the pattern-induced capacitance C_g. From the found impedance of patterned graphene, Faraday rotation is trivially found by analytically solving the boundary conditions at the interface.

Figure 1(c) compares the experimental data measured at $B = 7$ T with the calculated FR using an approximated analytical formula for C_g of the considered pattern given in Ref. [23]. A very good agreement is reached for the whole frequency range using $E_F = 0.43$ eV and $\tau = 44$ fs, thus capturing the magnetic-field-independent resonance frequency ω_F and bandwidth [from $\omega_F - (2\tau)^{-1}$ to $\omega_F + (2\tau)^{-1}$]. To illustrate the shift of the FR above the cyclotron resonance, the black curve in Fig. 1(c) is the calculated FR for continuous graphene using Eq. (1) and the extracted Fermi energy and scattering time. This allows us to see that the model also captures the amplitude of the FR and shows that, apart from the correction factor $p_{GSD} \approx 0.6$ which decreases the total Faraday rotation, patterned graphene retrieves the optimal Faraday rotation condition at the resonance frequency (found in uniform graphene for $\omega = 0$), namely,

$$Z_{M\pm}(\omega = \omega_F) = p^{-1} Z_{\pm}(\omega = 0). \quad (4)$$

Importantly, as shown in Fig. 1(d), this tells us that, as long as the factor ratio p is conserved, the amplitude of the Faraday rotation will be unchanged by a variation of the period P.

Because C_g is proportional to P [23], the resonance frequency ω_F can be easily tuned over a large portion of the THz range without any loss of FR, and this is independently of the cyclotron resonance energy.

The main drawback of the GSD structures is that once fabricated, no *in situ* tuning of the FR is possible: first, because the resonance frequency is magnetic field independent, and second, because as a noncontinuous graphene structure the Fermi level cannot be changed using a back gate. To overcome these limitations, in the following we will focus on structures allowing more flexibility.

Figure 2(a) is a SEM image of a typical GSA sample, with an antidot diameter $D = 4\ \mu$m and a periodicity $P = 6\ \mu$m. The apparent electrical continuity of this sample allows us to apply a gate voltage.

Figure 2(b) shows the Faraday rotation measured on GSA sample at gate voltage of $V_G = 136$ V (with respect to the charge neutrality point), corresponding to $E_F = 0.356$ eV. As the magnetic field increases, $\theta_F(\omega)$ displays a very different behavior from the one observed above, with two main features: a monotonic increase of the FR towards dc frequency and a local maximum of the FR centered around 3 THz (see red arrow). This behavior can be understood by considering a superposition of the two behaviors described in the first part of this Rapid Communication: (i) The GSA is an electrically continuous structure and as such Dirac carriers are free to move, thus the FR presents a maximum at zero energy (similar to the one observed in continuous graphene); (ii) plasmonic resonances take place in this structure due to Bragg scattering on the periodic structure [20], and when it becomes coupled with the cyclotron resonance, an enhancement of the FR is to be expected (and it is observed in the GSD structures). As B increases, both maxima increase in amplitude, reaching 2° for peak A and nearly 3° for peak B at $B = 7$ T. It is interesting to note that with similar filling factors ($p_{GSA} = 0.65$) both GSA and GSD present similar performances.

For a further understanding of this system, we performed finite-element electromagnetic simulations. The resulting numerical curves are shown in Fig. 2(c), demonstrating very good agreement with the experimental data. The shape, amplitude, and frequency of the resonance are all well reflected by the simulation, for all magnetic fields. From this fit we can extract an average scattering time of $\tau = 80$ fs, making the comparison with the previous structure even more relevant.

Let us now consider the *in situ* tuning capabilities of this structure. Figure 2(d) shows the FR measured at 7 T for four different values of the Fermi level. As the Fermi level moves closer to the Dirac point, the FR starts to decrease. $\theta_F(\omega)$ peaks at 2° for $E_F = 0.25$ eV and reaches a value close to zero for the whole experimental frequency range at $E_F = 0.07$ eV. Two phenomena take place simultaneously as E_F decreases: (i) The density of the carrier decreases, and the interaction between light and graphene becomes weaker, causing a smaller amplitude of the Faraday rotation, and (ii) the cyclotron resonance moves to a higher energy, raising as well the magnetoplasmon resonance. Figure 2(e) shows the simulated $\theta_F(\omega)$ for all the measured Fermi levels at a constant scattering time $\tau = 80$ fs. The simulations clearly show that the value of the maximum FR shifts from 4 up to 15 THz as the Fermi level is decreased. It can be seen that the experimental

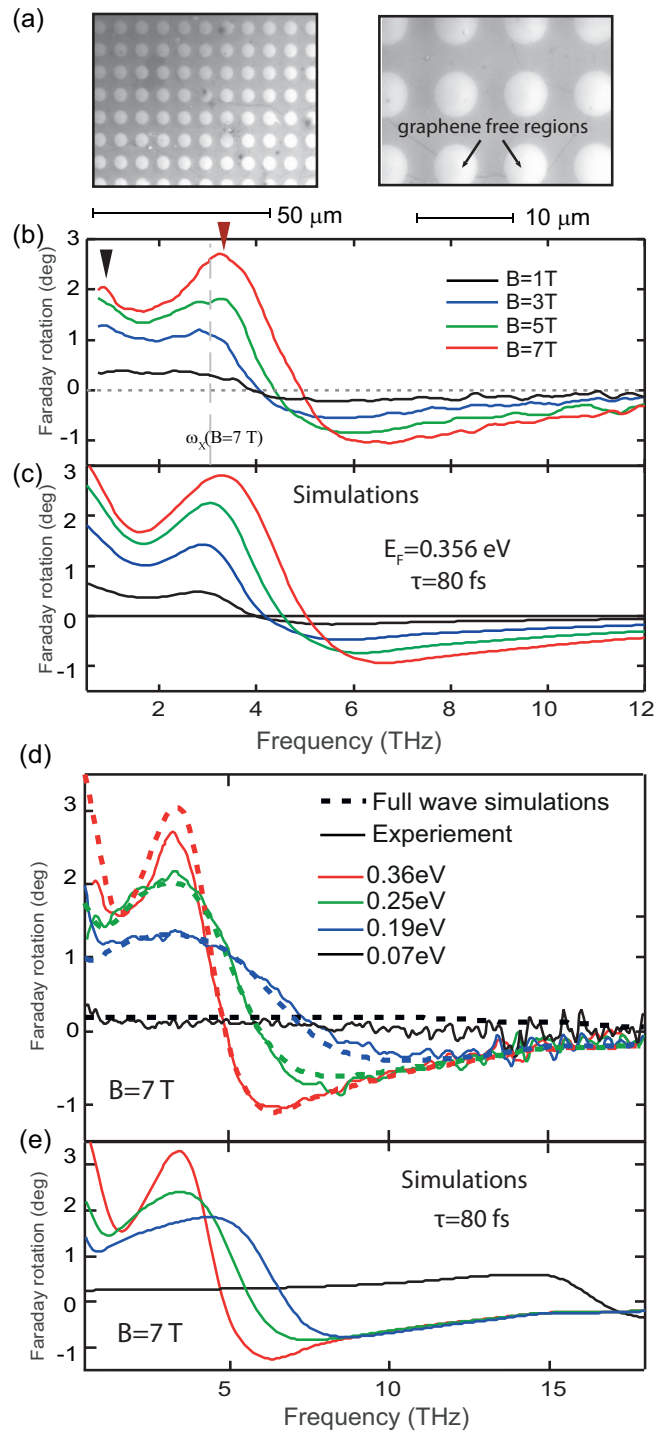

FIG. 2. (a) SEM pictures of the nanopatterned graphene square antidot lattice (GSA) sample studied in this work. $P = 6\ \mu$m, $D = 4\ \mu$m. (b) Measured Faraday rotation on the GSA sample at several magnetic fields up to 7 T. Expected ω_c in this system at $B = 7$ T is shown as a gray dashed line. (c) Simulated Faraday rotation for GSA with $\tau = 80$ ps and $E_F = 0.356$ eV. (d) Solid lines: Faraday rotation measured at $B = 7$ T for different values of the E_F. Dashed line: Full-wave simulations for the FR for fixed mobility $\mu = 2500\ \text{cm}^2/(\text{V s})$ calculated for the corresponding value of E_F. (e) Simulated Faraday rotation measured at $B = 7$ T for fixed $\tau = 80$ fs.

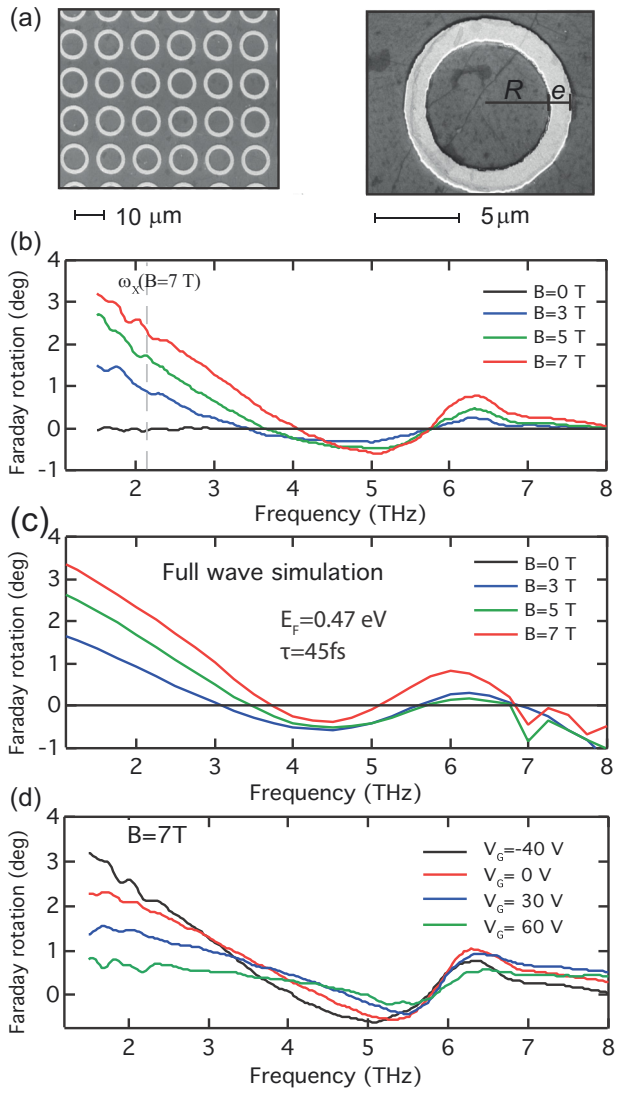

FIG. 3. (a) SEM pictures of the hybrid metal-graphene sample (HMG) sample $R = 4\ \mu$m, $e = 1\ \mu$m, $P = 13\ \mu$m. (b) Measured Faraday rotation at various fields, up to 7 T, for a fixed back gate voltage $V_G = 50$ V. Expected ω_c in this system at $B = 7$ T is shown as a gray dashed line. (c) Fit of the measurements with numerical full-wave simulations, for $E_F = 0.47$ eV and $\tau = 45$ fs. (d) Faraday rotation measured at $B = 7$ T for different values of V_G.

data do not show the same behavior, with no evidence of FR resonance for $E_F = 0.07$ eV. Trying to reproduce the experimental data, we realized that the scattering time is not a good fitting parameter, because as the Fermi energy decreases, the effective mass of the graphene carriers changes, $m = E_F/v_F^2$. The dashed lines in Fig. 2(d) show the simulated FR for all measured Fermi energies, taking into account a constant mobility $\mu = \tau/m = 2500\ \mathrm{cm}^2/(\mathrm{V\,s})$ instead of a constant scattering time. One can see that this fitting procedure allows a very good agreement with the experimental data and gives a gate efficiency for this system $C_G = 6.9 \times 10^{12}\ \mathrm{cm}^{-2}/\mathrm{V}$.

Finally, the last structure studied in this Rapid Communication is a periodic square lattice of gold rings covered by uniform monolayer graphene, as shown in Fig. 3(a). The gold layer of 100 nm is evaporated directly on the silicon oxide and the graphene layer is transferred on it afterwards. The radius of the ring is $R = 4\ \mu$m, the ring width $e = 1\ \mu$m, and the pattern has a periodicity $P = 13\ \mu$m. An obvious advantage of such an HMG patterned structure is that no part of the surface graphene is removed. Consequently, the Fermi level can be tuned via the gate voltage.

Figure 3(b) shows the results of the FR measurement for the HMG at a fixed back gate voltage $V_G = -40$ V for magnetic fields up to 7 T. Similarly to the previous system, two clear features appear in $\theta_F(\omega)$: The dc resonance is due to the free carriers and the magnetoplasmonic resonance in this case lies at 6.3 THz. The value of the maximum Faraday rotation for peak B increases with increasing magnetic field and reaches almost 1° at $B = 7$ T.

Results of the full-wave simulations are shown in Fig. 3(c). To simplify the calculations, Maxwell's equations were not solved inside the gold, which was approximated as a thin-film impedance. The presence of the gold rings in the vicinity of graphene affects the local electric field increasing it at the center of the ring. Graphene interacts with the enhanced field, and the equivalent conductivity of graphene at this frequency becomes different for the left- and right-handed circular polarizations, causing Faraday rotation to appear.

It can be seen that the model accounts well for the amplitude and frequency of both the experimentally observed modes. Interestingly, to reach such an agreement with the experimental data, the conductivity of the gold rings has to be decreased with respect to the nominal value. This is probably due to either discontinuities in the gold rings because of imperfect fabrication or to strong skin depth effects in metal at these frequencies. This may explain why, among the studied structures, the HGM structure presents the smallest enhancement of Faraday rotation of the studied structures. We believe that an improved fabrication process could result in better performances and would enable the structure to reach values of Faraday rotation similar to the two previous metastructures. One can also see that the simulation predicts the presence of a third peak above 7 THz that appears clearly above 3 T, a resonance that appears in the experimental data as a shoulder above the second resonance.

Figure 3(d) shows the FR measurement at constant magnetic field and for several gate voltages. Contrary to what has been observed in GSA, where the resonance frequency is tuned by the carrier density, the resonance frequency is fixed in the HGM structures. The numerical model shows that the metallic pattern sets its own resonance frequency and dominates the response of the system. Hence, the resonance frequency does not appreciably depend on the charge carrier density in the graphene layer. Instead, the amplitude of the rotation is strongly affected by the carrier density, hence decoupling these two degrees of freedom.

In conclusion, we have demonstrated that, by using three different types of metasurfaces, the Faraday rotation in graphene can be extended to the high terahertz band and potentially to the mid-IR, independently of the cyclotron resonance energy, thus paving the way for different nonreciprocal devices based on graphene. The GSD array presents a resonant behavior acting in a specific frequency band. The frequency is adjustable over a large range of THz frequencies, in principle, without any losses in the Faraday rotation. The

GSA array shows similar performances reaching 3° of Faraday rotation, but on a broader frequency range due to multiple resonance frequencies. The amplitude and frequency of these resonances can be tuned using the gate voltage. Finally, the HMG metasurface allows us to decouple the frequency from the amplitude tuning.

This work has been financially supported by the Swiss National Science Foundation (SNSF) under Grants No. 133583 and No. 168545, the Hasler Foundation under Project No. 11149, and the European Commission under Graphene Flagship (Contract No. CNECT-ICT-604391). We gratefully acknowledge discussions with Dr. Daniel Rodrigo Lopez.

[1] V. P. Gusynin, S. G. Sharapov, and J. P. Carbotte, J. Phys.: Condens. Matter **19**, 026222 (2007).
[2] G. W. Hanson, IEEE Trans. Antennas Propag. **56**, 747 (2008).
[3] I. Crassee, J. Levallois, A. L. Walter, M. Ostler, A. Bostwick, E. Rotenberg, T. Seyller, D. van der Marel, and A. B. Kuzmenko, Nat. Phys. **7**, 48 (2011).
[4] I. Crassee, M. Orlita, M. Potemski, A. L. Walter, M. Ostler, T. Seyller, I. Gaponenko, J. Chen, and A. B. Kuzmenko, Nano Lett. **12**, 2470 (2012).
[5] A. Fallahi and J. Perruisseau-Carrier, Appl. Phys. Lett. **101**, 231605 (2012).
[6] D. L. Sounas and C. Caloz, IEEE Trans. Microwave Theory Tech. **60**, 901 (2012).
[7] D. Sounas and C. Caloz, *Novel Electromagnetic Phenomena in Graphene and Subsequent Microwave Devices Enabled by Multi-Scale Metamaterials* (InTech, Rijeka, Croatia, 2012).
[8] H. Yan, Z. Li, X. Li, W. Zhu, P. Avouris, and F. Xia, Nano Lett. **12**, 3766 (2012).
[9] M. Shalaby, M. Peccianti, Y. Ozturk, and R. Morandotti, Nat. Commun. **4**, 1558 (2013).
[10] R. Shimano, G. Yumoto, J. Y. Yoo, R. Matsunaga, S. Tanabe, H. Hibino, T. Morimoto, and H. Aoki, Nat. Commun. **4**, 1841 (2013).
[11] D. L. Sounas, H. S. Skulason, H. V. Nguyen, A. Guermoune, M. Siaj, T. Szkopek, and C. Caloz, Appl. Phys. Lett. **102**, 191901 (2013).
[12] N. Ubrig, I. Crassee, J. Levallois, I. O. Nedoliuk, F. Fromm, M. Kaiser, T. Seyller, and A. B. Kuzmenko, Opt. Express **21**, 24736 (2013).
[13] M. Tymchenko, A. Y. Nikitin, and L. Martín-Moreno, ACS Nano **7**, 9780 (2013).
[14] X. Lin, Z. Wang, F. Gao, B. Zhang, and H. Chen, Sci. Rep. **4**, 4190 (2014).
[15] Y. Hadad, A. R. Davoyan, N. Engheta, and B. Z. Steinberg, ACS Photonics **1**, 1068 (2014).
[16] M. Tamagnone, A. Fallahi, J. R. Mosig, and J. Perruisseau-Carrier, Nat. Photonics **8**, 556 (2014).
[17] H. S. Skulason, D. L. Sounas, F. Mahvash, S. Francoeur, M. Siaj, C. Caloz, and T. Szkopek, Appl. Phys. Lett. **107**, 093106 (2015).
[18] M. Tamagnone, C. Moldovan, J.-M. Poumirol, A. B. Kuzmenko, A. M. Ionescu, J. R. Mosig, and J. Perruisseau-Carrier, Nat. Commun. **7**, 11216 (2016).
[19] G. F. Dionne, G. A. Allen, P. R. Haddad, C. A. Ross, and B. Lax, Lincoln Lab. J. **15**, 323 (2005).
[20] P. Q. Liu, F. Valmorra, C. Maissen, and J. Faist, Optica **2**, 135 (2015).
[21] H. Yan, T. Low, W. Zhu, Y. Wu, M. Freitag, X. Li, F. Guinea, P. Avouris, and F. Xia, Nat. Photonics **7**, 394 (2013).
[22] J. Levellois, I. O. Nedoliuk, I. Crassee, and A. B. Kuzmenko, Rev. Sci. Instrum. **86**, 033906 (2015).
[23] L. B. Whitbourn and R. C. Compton, Appl. Opt. **24**, 217 (1985).
[24] C. Balanis, *Antenna Theory: Analysis and Design* (Wiley, Hoboken, NJ, 2005), Vol. 1, Chap. 12, Table 12.1.